

Size effects in the ultrafast electronic dynamics of metallic tin nanoparticles

A. Stella

Dipartimento di Fisica "Alessandro Volta," Università degli Studi, Pavia, Italy

M. Nisoli, S. De Silvestri, and O. Svelto

Centro di Elettronica Quantistica e Strumentazione Elettronica-CNR, Dipartimento di Fisica, Politecnico, Milano, Italy

G. Lanzani

Istituto di Matematica e Fisica, Università di Sassari, Sassari, Italy

P. Cheyssac and R. Kofman

Laboratoire de Physique de la Matière Condensée, URA 190, Université de Nice Sophia Antipolis, Nice Cedex, France

(Received 29 February 1996)

We report on femtosecond transient reflectivity measurements performed on metallic tin nanoparticles, embedded in an Al_2O_3 matrix, with average radii in the range 20–60 Å. It was observed that the time behavior of the transient reflectivity decays depends upon particle size. The results can be interpreted in terms of a size-dependent electron-surface interaction in the thermalization process and of a substantially size-independent electron-electron thermalization. [S0163-1829(96)04723-6]

Clusters and aggregates of atoms in the nanometer size range (currently called nanoparticles) are systems somewhat intermediate in several respects between simple molecules and bulk materials, and have been the object of intensive work particularly in the case of semiconductors quantum dots.¹ We shall confine our attention to metallic nanoparticles, which have been the object of recent work also for what concerns ultrafast dynamics.^{2–4} The main motivation for the growing interest in these systems is related to the possibility of tailoring, to a considerable extent, their physical behavior on the basis of size. As a matter of fact, when the size becomes smaller than 10 Å relevant quantum effects show up,^{5–7} giving rise to a large discretization in the distribution of the electronic levels. Above that size the width of the discrete levels becomes comparable to or larger than the separation between them, so that we are in a regime where the conduction band is quasicontinuous⁶ and the behavior of the nanoparticles tends to approach that of the bulk metal, presenting, however, some significant differences concerning, for instance, thermodynamic properties (such as decrease of melting temperature with size^{8,9}) and nonlinear effects in the optical spectra.¹⁰ In this intermediate size range a careful investigation of the role of particle dimensions on the electron relaxation dynamics appears to be essential in order to improve our knowledge of the basic properties of metal nanoparticles as compared to bulk.

In this paper we present experimental results, which give evidence of the role of size in affecting the ultrafast electron relaxation dynamics in metal nanoparticles. The experiments have been performed on tin nanocrystals with radii in the range 20–60 Å by the femtosecond transient reflectivity technique. The size values considered here are above 10 Å on one side and below 80 Å on the other side, where more complex phenomena due to generation and propagation of shock waves can take place.¹¹

The samples were prepared by evaporation condensation of high purity materials in ultrahigh vacuum on carefully cleaned substrates of sapphire.¹² Sn vapor was condensed on a previously evaporated film of Al_2O_3 ~40 Å thick, so that nucleation and growth of the particles could occur in the liquid state, by keeping the substrate temperature sufficiently high. The population of the Sn grains was then quenched and subsequently covered and protected by an additional layer of Al_2O_3 ~100 Å thick. The final product was given by Sn nanocrystals with radii obtainable in a wide range and embedded in a dielectric matrix, with size dispersion $\leq 20\%$ and shape of truncated spheres as expected from the fact that Sn does not wet Al_2O_3 . From the contact angle Sn- Al_2O_3 ~114° it was calculated that the volume of the truncated spheres is 80% of that of ideally perfect spheres with the same radius. The size distribution was found typically bimodal, 95% peaking around the average radius with a polydispersed tail toward zero radius.¹³ As far as the density of nanoparticles is concerned, the filling factor was always smaller than 0.3, so that all experiments were performed in the Maxwell-Garnett regime. Their good crystalline nature was clearly shown by means of electron microscopy¹² in the dark field configuration, where oriented particles satisfying the Bragg condition appeared uniformly bright in correspondence with the (200) ring of the diffraction pattern of the β -tetragonal phase. In addition, no impurities or defects were detected. The measurements were performed on three tin samples with radii of 20, 40, and 60 Å. The corresponding transmission spectra are shown in Fig. 1.¹⁴ Note that the plasmon peak, which is the dominant structure of metallic nanoparticles, is expected to fall at a frequency $\omega^* = \omega_p / \sqrt{1 + 2\epsilon_r}$ (where ω_p is the bulk plasma frequency ~14 eV for metallic tin,¹⁵ and ϵ_r is the relative dielectric constant of the matrix), i.e., ~200 nm, this wavelength being shorter than those of the pump-probe experiments. The excitation takes place on the low-energy side of the peak of the broad unstructured collective resonance.¹⁶

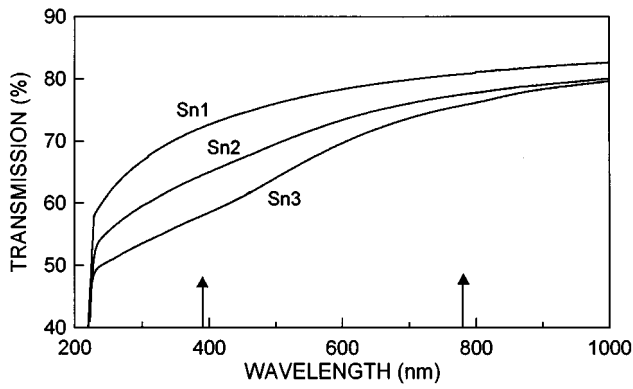


FIG. 1. Transmission spectra of the samples Sn1, Sn2, Sn3, with radii 20, 40, and 60 Å, respectively. The evolution towards the plasmon peak is evident. The cutoff on the shorter wavelength side is due to the absorption of the sapphire substrate. The arrows indicate the pump pulse wavelengths used in the experiments.

Transient reflectivity measurements were performed using a conventional pump-probe configuration. The laser system consists of a Ti:sapphire laser with chirped pulse amplification, which provides pulses of 150-fs duration at 780 nm with energy up to 750 μJ at 1-kHz repetition rate. In the transient nondegenerate experiments pump and probe wavelengths were 390 and 780 nm, respectively. The pump beam was obtained by frequency doubling a fraction of the laser beam in a LiB_3O_5 crystal of 1-mm length. The pump pulse duration was 180 fs and the energy used in the measurements was in the range 6–60 nJ. The pump and probe beams were focused onto the sample to focal spots with diameters of ~ 250 and 100 μm , respectively. The pump beam was chopped at 400 Hz and the signal was detected using a lock-in amplifier. Degenerate transient reflectivity measurements were performed on a subpicosecond time scale by using ultrashort pulses at 780 nm, obtained by a compression technique.¹⁷ The 150-fs pulses were focused in a hollow core fused silica wave guide (140- μm bore diameter), filled with krypton at 2-atm pressure to broaden the spectrum mainly by self-phase modulation. The frequency-chirped pulses were then compressed with two quartz prism pairs. Pulses of 10-fs duration with energy up to 240 μJ and almost transform limited were obtained. Pump and probe beam polarizations were made orthogonal to avoid thermal grating buildup. The transient reflectivity changes ΔR in samples containing nanoparticles of different size (Sn1, 2, and 3 in Table I) are shown in Fig. 2(a) as a function of probe time delay, for pump and probe wavelengths at 390 and 780 nm, respectively. The transient reflectivity curves show a rise time that

TABLE I. Values of the time constants (τ_1, τ_2, τ_3), obtained from the fitting of transient reflectivity measurements in the three investigated samples.

Sample	Radius (Å)	Time constants		
		τ_1 (ps)	τ_2 (ps)	τ_3 (ps)
Sn1	20	0.62	12	580
Sn2	40	1.05	16.7	300
Sn3	60	1.42	22.7	460

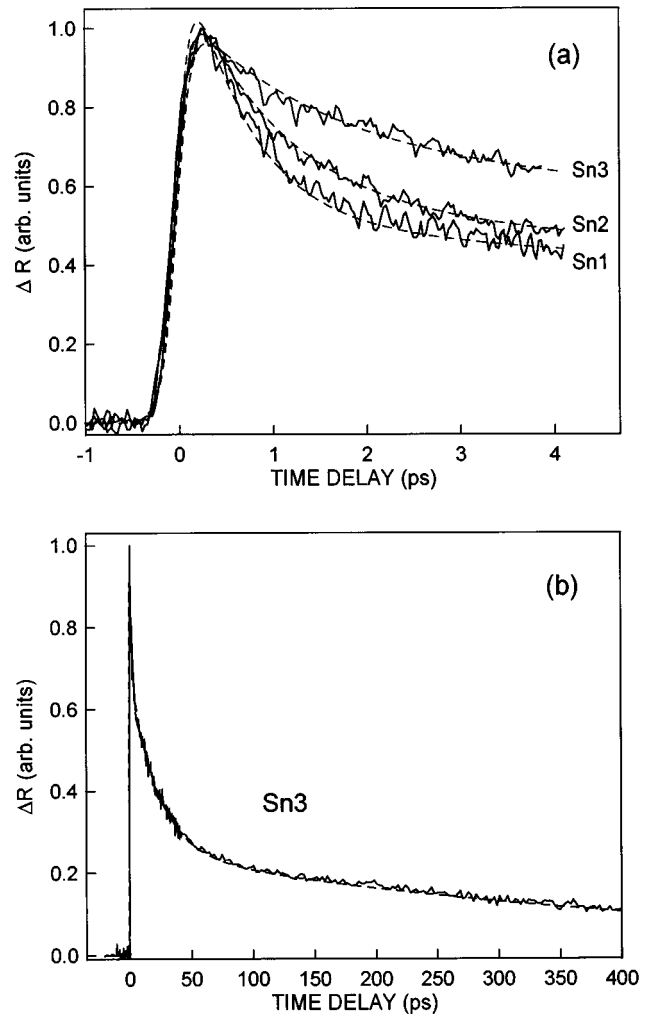


FIG. 2. (a) Transient reflectivity changes ΔR in Sn1, 2, and 3, as a function of probe time delay ($\lambda_{\text{pump}}=390$ nm, $\lambda_{\text{probe}}=780$ nm); the dashed lines are the fitting curves; (b) ΔR in Sn3 on an extended time scale, the dashed line is the fitting curve (the sampling density has been increased for small time delay to show the actual time decay).

follows the time integral of the pump-probe intensity cross-correlation function and an initial fast decay that shows a particle size dependence. The temporal behavior of the data measured for Sn3 is reported in Fig. 2(b) on an extended time scale. A simple analysis of the transient reflectivity curve of Fig. 2(b) provides evidence of the separation of the decay into three distinct time scales. A similar time evolution was observed in the data measured for Sn1 and Sn2. Characteristic time constants can be assigned to each time scale if the curves are fitted by a three exponential function. The values of the time constants τ_1 , τ_2 , and τ_3 , as obtained by the fitting, are given in Table I for the different samples. It is worth noting that the three time constants are largely different, giving additional support to the validity of the results obtained from the fitting. The three τ 's are indicative of three different processes, as discussed below.

In the nanoparticles the energy transfer from the laser to the electron gas occurs mainly through excitation of the broad plasmon mode and the superimposed single electron modes,^{6,16} whereas the contribution due to interband transi-

tions is expected to be negligible.¹⁸ In the size range of the nanoparticles explored here the transient reflectivity data can be interpreted in the framework of the electron relaxation model developed for bulk metals, pointing out the effects arising from the electron confinement in the nanometer structures. During the femtosecond pump pulse a change is induced in the electron energy distribution due to the formation of a low-density nonthermalized highly energetic electron population. The acquired energy is redistributed by electron-electron collisions and electron-phonon collisions. The electron thermalization usually occurs on a subpicosecond time scale, therefore, a hot Fermi distribution with a temperature $T_e > T_o$ (where T_o is the initial sample temperature) is formed. The hot electron system thermalizes with the lattice by electron-phonon collisions and interactions with the nanoparticle surface, as well as with defects and impurities (if present). The electron-lattice thermalization process, investigated extensively in bulk metals, usually occurs on a time scale of a few picoseconds.^{19–21} The excess thermal energy in the nanoparticles is then removed by thermal diffusion toward the matrix. This process occurs on a time scale typically of the order of tens of picoseconds. Finally on a time scale of hundreds of picoseconds the whole ensemble nanoparticle matrix reaches the initial temperature of the sample. The electron-electron and electron-lattice relaxation processes in bulk have been analyzed by making use of a rate equation model reported in detail in Ref. 22. In the low perturbation limit, this model can provide a response function of the transient reflectivity change given by simple exponential functions under the assumptions that the lattice heat capacity is much greater than electronic heat capacity and that the electronic heat capacity is almost temperature independent.

The time constants τ_1 reported in Table I for the different Sn nanoparticles, under excitation at 390 nm, can be associated to the process of thermalization of the hot electron Fermi distribution with the lattice. This process, usually dominated in bulk by electron-phonon collisions, may undergo substantial variations in nanoparticles. If the radius of the metal nanospheres is comparable with the electron mean free path, the electron-surface interactions cannot be neglected. Actually, the presence of the surface may be essential in determining the eigenstates within the nanocrystal volume.⁷ A suitable theoretical study of this issue is far from being trivial and goes beyond the scope of the present work. However, here we show that an approach based on a surface limited mean free path effect already yields interesting results. From the dc resistivity of tin it is possible to estimate an electron-phonon collision time $t_b \sim 2.3$ fs.²³ The mean free path of the conduction electrons in the bulk is thus given by $l_b = v_F t_b \sim 44$ Å, where v_F is the Fermi velocity ($v_F \sim 1.9 \times 10^8$ cm/s in tin²³). Therefore in the nanoparticles investigated here the electron collisions with the surface play an important role. The mean free path determined only by collisions with the surfaces of a spherical particle is equal to the particle radius R (assuming diffuse electron reflections at the surface),²⁴ so that the collision time is given by R/v_F .^{7,25} Taking into account the surface contribution to the electronic population relaxation, the time constant τ_1 can be written as follows:

$$\frac{1}{\tau_1} = \frac{1}{\tau_0} + \frac{v_F}{\alpha R}, \quad (1)$$

where τ_0 is a size-independent time constant, which includes all the energy relaxation processes different from the electron-surface scattering, and α is the average number of collisions, which are effective for obtaining electron energy relaxation by surface interaction. The relation between τ_1 and R observed in our pump-probe measurements on Sn1, 2, and 3 is well fitted by Eq. (1) with $\alpha \sim 700$ and $\tau_0 \sim 3.8$ ps, indicating that the surface effects play a role. The fitting was performed under the assumption (which appears to be reasonable in our size range) that the Fermi velocity is not appreciably altered by space confinement. We have verified that the hot-electron lifetime τ_1 does not depend on the excitation laser fluence in the interval 12–120 $\mu\text{J}/\text{cm}^2$ and the peak value $\Delta R/R$ varies linearly in this range $5 \times 10^{-4} - 5 \times 10^{-3}$. Assuming that all the absorbed energy ($\sim 5\%$ of the input energy) is initially stored into the thermalized electron gas, we can estimate that the electron temperature variation is in the range $\Delta T_e \sim 32 - 320$ K, indicating that the measurements were performed in the low perturbation limit.

The relaxation dynamics on the longer time scale is described through the time constants τ_2 and τ_3 (see Table I). The particle-size dependence of τ_2 can be explained on the basis of the following considerations: the total absorbed energy per particle is proportional to its volume, while the heat dissipation is proportional to the surface area, so that a thermal buildup for the larger particles is produced.² The temperature rise of the lattice has been estimated not to exceed 5 K. The size dependence of τ_2 can be associated to the heat transfer from the nanoparticle to the matrix: we obtain longer τ_2 for the bigger particles. The time constant τ_3 can be related to the process of cooling of the ensemble nanoparticle matrix to the initial temperature, and it is not expected to exhibit a strong dependence on the particle size.

To investigate the subpicosecond electron-electron thermalization dynamics in nanoparticles, we have performed degenerate pump-probe measurements using 10-fs pulses at

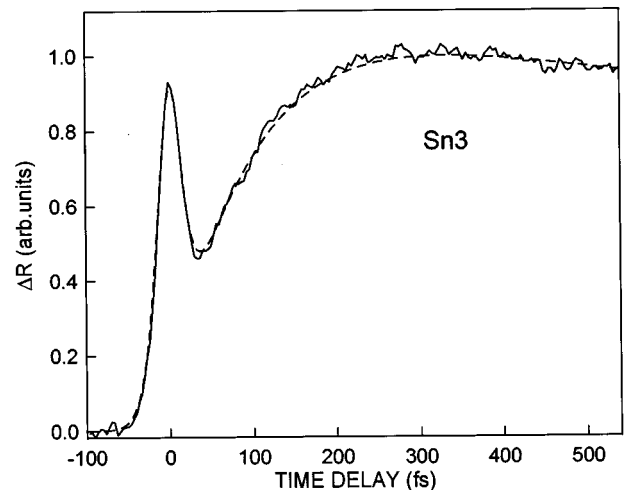


FIG. 3. Degenerate transient reflectivity change ΔR in Sn3 as a function of probe time delay ($\lambda_{\text{pump}} = \lambda_{\text{probe}} = 780$ nm); the dashed line is the fitting curve.

780 nm. The transient reflectivity change, reported in Fig. 3 for Sn3, shows a rise time characterized by a time constant of 100 fs, which describes the buildup of the hot Fermi distribution through electron-electron interactions. We have verified that the rise time is substantially constant in the size range from 20 to 60 Å. The electron thermalization time is also quite independent on the laser fluence in the range 30–300 $\mu\text{J}/\text{cm}^2$. This can be explained taking into account the small fraction of the input energy absorbed by the nanoparticles. In this case the temperature of the thermal part of the electronic distribution does not substantially increase. Therefore the number of hot electrons with which the nonthermal electrons can scatter is quite constant. Moreover, due to the low perturbation regime of our experiments, the thermal component never overtakes or overlaps the nonthermal part of the electronic distribution.²⁶

In conclusion, we have reported experimental evidence of a size-dependent electron relaxation process in metallic tin nanoparticles in a size range where a comparison with the bulk can be carried out. In particular, novel information is achieved: (i) electron-surface interaction cannot be neglected with respect to other scattering mechanisms and specifically the typical bulk electron-phonon scattering; (ii) the fast rise time of the transient reflectivity can be attributed to electron-electron interaction characterized by a size independent time constant of 100 fs.

The useful assistance of Dr. A. Migliori and Dr. P. Tognini for electron microscopy and optical characterization is gratefully acknowledged. This work was partially supported by the National Research Council and the Ministry of Scientific and Technological Research.

-
- ¹L. Banyai and S. W. Koch, *Semiconductor Quantum Dots* (World Scientific, Singapore, 1993), and references therein.
- ²M. J. Bloemer, J. W. Haus, and P. R. Ashley, *J. Opt. Soc. Am. B* **7**, 790 (1990).
- ³K. Uchida, S. Kaneko, S. Omi, C. Hata, H. Tanji, Y. Asahara, J. Ikushima, T. Tokizaki, and A. Nakamura, *J. Opt. Soc. Am. B* **11**, 1236 (1994).
- ⁴T. W. Roberti, B. A. Smith, and J. Z. Zhang, *J. Chem. Phys.* **102**, 3860 (1995).
- ⁵A. Kawabata and R. Kubo, *J. Phys. Soc. Jpn.* **21**, 1765 (1966).
- ⁶U. Kreibig, *J. Phys. F* **4**, 999 (1974).
- ⁷D. M. Wood and N. W. Ashcroft, *Phys. Rev. B* **25**, 6255 (1982).
- ⁸R. Kofman, P. Cheyssac, A. Aouaj, Y. Lereah, G. Deutscher, T. Ben David, J. M. Penisson, and A. Bourret, *Surf. Sci.* **303**, 231 (1994).
- ⁹F. Ercolessi, W. Andreoni, and E. Tosatti, *Phys. Rev. Lett.* **66**, 911 (1991).
- ¹⁰F. Hache, D. Ricard, C. Flytzanis, and U. Kreibig, *Appl. Phys. A* **47**, 347 (1988).
- ¹¹This takes place when the light penetration depth is smaller than the particle size [S. De Silvestri, M. Nisoli, and A. Stella (unpublished)].
- ¹²P. Cheyssac, R. Kofman, G. Mattei, P. G. Merli, A. Migliori, and A. Stella, *Superlatt. Microstruct.* **17**, 47 (1995); A. Stella, P. Cheyssac, R. Kofman, and A. Migliori, *Europhys. Lett.* **26**, 265 (1994).
- ¹³This presents interesting similarities with results obtained for the growth of semiconductor quantum dots with different techniques. See, e.g., D. Leonard, M. Krishnamurthy, C. M. Reaves, S. P. Denbaars, and P. M. Petroff, *Appl. Phys. Lett.* **63**, 3203 (1993); J. M. Moison, F. Houzay, F. Barthe, and L. Leprince, *ibid.* **64**, 196 (1994).
- ¹⁴It is worth noting that both energy resolution of the apparatus (a few meV) and density of the particles are suitable for a quite detailed investigation of spectral structures [see, e.g., R. W. Cohen, G. D. Cody, M. D. Coutts, and B. Abeles, *Phys. Rev. B* **8**, 3689 (1973); D. Aspnes, *Thin Solid Films* **89**, 249 (1982)].
- ¹⁵R. A. MacRae, E. T. Arakawa, and M. W. Williams, *Phys. Rev.* **162**, 615 (1967).
- ¹⁶W. Ekart, *Phys. Rev. B* **31**, 6360 (1985).
- ¹⁷M. Nisoli, S. De Silvestri, and O. Svelto, *Appl. Phys. Lett.* (to be published).
- ¹⁸The role of interband transitions is expected to be negligible in the same energy range also in bulk tin [see, e.g., L. Viña, H. Höchst, and M. Cardona, *Phys. Rev. B* **31**, 958 (1985)], where, however, free carrier absorption is due mainly to scattering with phonons.
- ¹⁹R. W. Schoenlein, W. Z. Lin, J. G. Fujimoto, and G. L. Eesley, *Phys. Rev. Lett.* **58**, 1680 (1987).
- ²⁰C.-K. Sun, F. Vallée, L. Acioli, E. P. Ippen, and J. G. Fujimoto, *Phys. Rev. B* **48**, 12 365 (1993).
- ²¹H. E. Elsayed-Ali and T. Juhasz, *Phys. Rev. B* **47**, 13 599 (1993).
- ²²C.-K. Sun, F. Vallée, L. H. Acioli, E. P. Ippen, and J. G. Fujimoto, *Phys. Rev. B* **50**, 15 337 (1994).
- ²³N. W. Ashcroft and N. D. Mermin, *Solid State Physics* (Holt-Saunders, Orlando, 1976).
- ²⁴J. Euler, *Z. Phys.* **137**, 318 (1954).
- ²⁵U. Kreibig and C. V. Fragstein, *Z. Phys.* **224**, 307 (1969).
- ²⁶W. S. Fann, R. Storz, H. W. K. Tom, and J. Bokor, *Phys. Rev. B* **46**, 13 592 (1992).